# Water Bending Mode at the Water–Vapor Interface Probed by Sum-Frequency Generation Spectroscopy: A Combined Molecular Dynamics Simulation and Experimental Study

**ARTICLE** *in* JOURNAL OF PHYSICAL CHEMISTRY LETTERS · JUNE 2013

Impact Factor: 7.46 · DOI: 10.1021/jz400683v



**6 AUTHORS**, INCLUDING:

Yuki Nagata
Max Planck Institute for Polymer Research
**33** PUBLICATIONS **324** CITATIONS
SEE PROFILE

Judith Voll
University of California, Irvine
**11** PUBLICATIONS **87** CITATIONS
SEE PROFILE

Mischa Bonn
Max Planck Institute for Polymer Research
**347** PUBLICATIONS **7,569** CITATIONS
SEE PROFILE

THE JOURNAL OF PHYSICAL CHEMISTRY Letters

Letter

pubs.acs.org/JPCL

# Water Bending Mode at the Water–Vapor Interface Probed by Sum-Frequency Generation Spectroscopy: A Combined Molecular Dynamics Simulation and Experimental Study

Yuki Nagata,*[,†] Cho-Shuen Hsieh,[†,‡] Taisuke Hasegawa,[§] Judith Voll,[†] Ellen H. G. Backus,[†] and Mischa Bonn*[,†]

[†]Max-Planck Institute for Polymer Research, Ackermannweg 10, 55128, Mainz, Germany

[‡]FOM-Institute AMOLF, Science Park 104, 1098 XG, Amsterdam, The Netherlands

[§]Max-Planck Research Department for Structural Dynamics, University of Hamburg, Center for Free Electron Laser Science, Luruper Chausee 149, 22607, Hamburg, Germany

Supporting Information

**ABSTRACT:** We present a combined molecular dynamics simulation and experimental study on the water bending mode at the water–vapor interface using sum-frequency generation (SFG) spectroscopy. The SFG spectrum simulated using an ab initio-based water model shows good agreement with the experimental data. The imaginary part of the SFG response shows a negative peak at ∼1650 $cm^{-1}$ and a positive peak at ∼1730 $cm^{-1}$. Our results reveal that these widely (∼80 $cm^{-1}$) separated peaks result from the interference of two closely spaced (∼29 $cm^{-1}$) peaks of opposite sign. The positive peak at ∼1689 $cm^{-1}$ originates from water with two donor hydrogen atoms with the HOH angular bisector pointing down toward the bulk, and the negative peak at ∼1660 $cm^{-1}$ from water with free O–H groups, pointing up. The small frequency difference of 29 $cm^{-1}$ indicates that the HOH bending mode frequency of interfacial water is relatively insensitive to the number of hydrogen bonds.

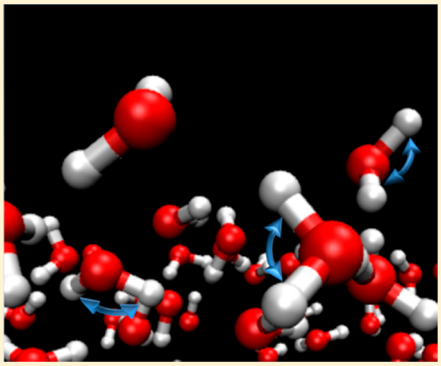

**SECTION:** Surfaces, Interfaces, Porous Materials, and Catalysis

Water in contact with hydrophobic interfaces constitutes a commonplace platform for chemical and biological processes.[1] The water–vapor interface is the simplest representative of water adjacent to a hydrophobic surface.[2−5] In addition to serving as a model system for aqueous hydrophobic interfaces, the water–vapor interface is directly relevant for atmospheric chemistry and physics. Revealing the structure and dynamics of interfacial water at the water–vapor interface is important for understanding the processes occurring at this interface. A key question regarding water at the water–vapor interface is the extent to which its structure and dynamics differ from those of bulk water.

Vibrational sum-frequency generation (SFG) spectroscopy is a powerful tool to probe the interfacial molecular response owing to its interface-sensitive property.[6] SFG signals generated by an infrared (IR) pulse and a visible pulse are enhanced by interfacial molecular vibrations when the IR frequency is resonant with the transition. The spectral intensity depends on the molecular organization and the net orientation along the surface normal as well as the density of transition dipole moments.[6,7] This technique has been extensively used to investigate the interfacial water structure at the water–vapor interface, using the O–H stretch vibration of interfacial water molecules as probes of the local water environment. The O–H stretch SFG spectrum at the water–vapor interface shows a sharp peak at ∼3700 $cm^{-1}$, and a broad peak ranging from 3100 to 3600 $cm^{-1}$, which are attributed to free O–H groups of interfacial water pointing toward the vapor region and the O–H groups interacting with other water molecules, respectively.[8−10] Further SFG studies of the O–H stretch mode have focused on the hydrogen bond (HB) strength of interfacial water[11,12] and have demonstrated, for instance, the enrichment of free O–H groups, relative to O–D groups, in HDO due to nuclear quantum effects.[13,14] Since the transition dipole moment vector of the HOH bending mode is nearly parallel to the bisector of the HOH angle, the SFG spectrum of the water bending mode, recently first reported by Vinaykin and Benderskii[15] and in combination band spectroscopy by Borguet et al.,[16] provides additional information on the interfacial water structure.

Probing the water bending mode is also important to understand vibrational energy relaxation pathways of the O–H stretch mode. Since the frequency of the O–H stretch mode (3100–3600 $cm^{-1}$) overlaps with the overtone of the HOH bending mode (fundamental at 1640 $cm^{-1}$) in bulk water, the

**Received:** March 28, 2013
**Accepted:** May 16, 2013
**Published:** May 16, 2013

   dx.doi.org/10.1021/jz400683v | J. Phys. Chem. Lett. 2013, 4, 1872−1877

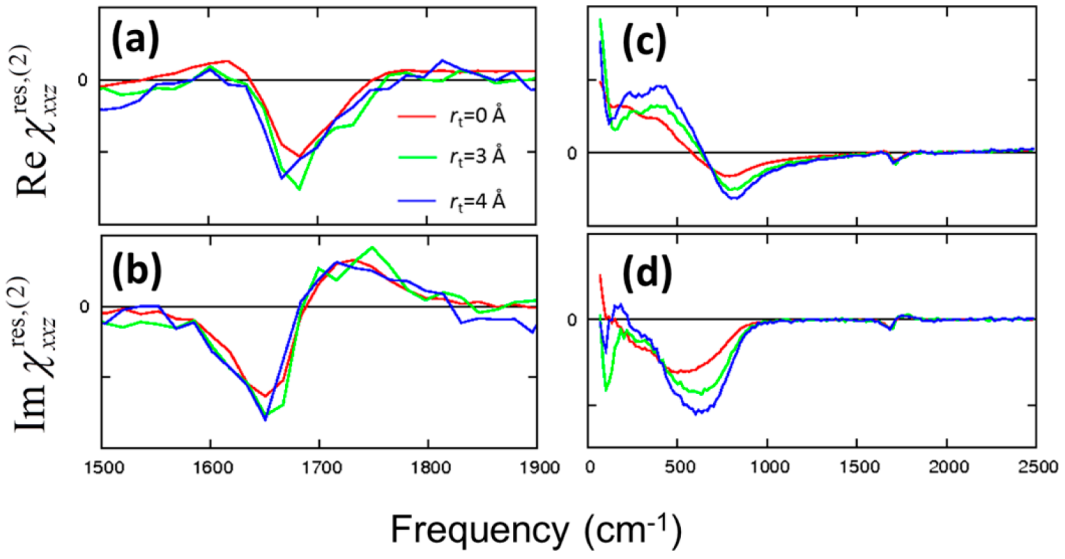


**Figure 1.** Simulated resonant part of (a,c) the real parts and (b,d) the imaginary parts of the SFG susceptibility.

excess energy of the stretch mode is mainly dissipated to the bending mode.[17−20] The vibrational energy relaxation lifetimes of the free O−H (O−D) stretch mode and the hydrogen bonded O−H (O−D) stretch mode at aqueous interfaces have been investigated using time- and polarization-resolved SFG and two-dimensional SFG spectroscopy,[21−27] while little information on the vibrational energy relaxation pathways has been obtained at the interfaces. Since the energy relaxation of the O−H stretch is sensitive to the frequency overlap between the O−H stretch and the HOH bending overtone modes, probing the HOH bending mode of interfacial water is essential.

Vinaykin and Benderskii inferred a prominent peak at 1656 cm$^{-1}$ and a small shoulder at 1750 cm$^{-1}$ as well as a low frequency peak at ∼1440 cm$^{-1}$ from the *ssp*-SFG spectrum of the HOH bending mode at the water−vapor interface.[15] Here, *ssp* denotes *s*-, *s*-, and *p*-polarization for the SFG signal, visible pulse, and IR pulse, respectively. Based on the empirical relation between the O−H stretch frequency ($\nu_{stretch}$) and the HOH bending mode frequency ($\nu_{bend}$) of water,[28]

$$\nu_{bend} = 1590 + 0.26(3705 - \nu_{stretch}) \quad (1)$$

the 1750 and 1656 cm$^{-1}$ HOH bending mode peaks were attributed to water contributing to the hydrogen bonded O−H stretch mode (3100−3500 cm$^{-1}$) and the free O−H stretch mode (∼3700 cm$^{-1}$), respectively. Equation 1 was previously obtained from IR spectra of various water-containing solids and liquids.[28] Since at the heterogeneous water−vapor interface the O−H stretch frequency is split into the frequencies associated with the free O−H stretch and hydrogen-bonded O−H stretch, it is not completely apparent that eq 1 obtained in homogeneous environments provides reliable peak assignments for the interfacial water HOH bending mode. Testing the peak assignments by using simulation techniques is, thus, helpful for advancing our understanding of the water bending mode SFG spectrum.

Molecular dynamics (MD) simulations have previously been performed to unveil the peak origins of the O−H stretch SFG spectrum,[7,10,12−14,29−41] while only one attempt for simulating the HOH bend SFG spectrum has been reported.[41] This may originate from the difficulty in modeling the HOH bending mode in bulk water; MD studies employing polarizable water models have shown that induced dipole moments critically affect the HOH bend peak shapes and intensity in the IR spectrum.[42,43] An accurate model of water accounting for induced dipole moments is required to reproduce the vibrational spectra of the bending mode. In this study, we use an ab initio-based polarizable force field model, which includes higher-order electric moment interactions up to quadrupole−quadrupole interactions.[42] This water model has successfully reproduced the vibrational IR and Raman spectra of the HOH bending mode.[42] We use it to calculate the water bend SFG spectra at the water−vapor interface and show that the simulated SFG intensity agrees well with the experimentally measured data. We analyze the contributions of the different types of interfacial water to the SFG spectra, which reveals the relation between the orientations of the HOH bend transition dipole moment and the imaginary part of the SFG response.

We simulated the resonant parts of the *xxz*-components of the SFG susceptibility of water HOH bend mode at the water−vapor interface based on the truncated cross-correlation function formalism:[32]

$$\chi^{res,(2)}_{xxz}(\omega; r_t) = iQ(\omega)\int_0^\infty dt e^{-i\omega t}\langle \sum_i g_{sc}^3(z_i(0))\mu_{i,z}(0)\alpha_{i,xx}(t) + \sum_i\sum_{j\neq i} g_{sc}(z_i(0))g_{sc}^2(z_j(0))\mu_{i,z}(0)\alpha_{j,xx}(t)g_t(r_{ij}(0); r_t)\rangle \quad (2)$$

where the first and second terms represent the autocorrelation and cross-correlation functions, respectively. $Q(\omega) = \beta\hbar\omega/(1 - \exp(-\beta\hbar\omega))$ is the harmonic quantum correction factor, with $\beta$ the inverse temperature, and $\mu_a(t)$ and $\alpha_{ab}(t)$ are the *a*-element of the molecular dipole moments and the *ab* tensor element of the molecular polarizability at time *t*, respectively. Note that several possible choices for the quantum correction are available,[44] but the results presented here are insensitive to the details of the correction. The function $g_{sc}$ inverts the molecular dipole moment near one of the two interfaces, while the function $g_t$ excludes the cross-correlation between molecules *i* and *j* if the intermolecular *i*−*j* distance is larger than the cutoff $r_t$. The details of the MD simulation and the


dx.doi.org/10.1021/jz400683v | J. Phys. Chem. Lett. 2013, 4, 1872−1877

methodology to calculate the SFG spectra are given in the Supporting Information. The water bend SFG responses for various values of the cross-correlation cutoff, $r_t$, are shown in Figure 1a,b. Both the imaginary and real parts of the SFG signals calculated with $r_t$ = 3 and 4 Å overlap with those calculated with $r_t$ = 0 Å, indicating that the water bend SFG signal originates mainly from the autocorrelation function, and the cross-correlation function has a small effect on the signal. This means that the water bend mode has very weak intermolecular couplings at the water−vapor interface. Although cross-correlations therefore do not affect the SFG bending mode response itself, these correlations are important to account for a contribution from the librational modes to the SFG intensity in the lower frequency part of the bending mode (1500−1700 $cm^{-1}$), as described in the following.

Figure 1c,d shows the simulated SFG susceptibility in the 100−1900 $cm^{-1}$ region. A broad SFG peak in the ∼700 $cm^{-1}$ region is observed, which mainly originates from the librational (rotational and translational) modes.[45] The long tail of this low frequency peak reaches the bending mode peak, in particular affecting the real part of the SFG susceptibility (Figure 1c). As the ∼700 $cm^{-1}$ mode is collective in nature, it is sensitive to cross-correlations, making the real part of the SFG susceptibility at bending mode frequencies depending on the cutoff $r_t$ (see Figure 1a). It seems evident that the 1440 $cm^{-1}$ peak used for the fitting in ref 15 represents the tail of the ∼700 $cm^{-1}$ peak.

To check the consistency of the simulated spectrum with the experimental data, the SFG intensity for the water bend mode at the *ssp* polarization was measured and was compared with the simulated resonant SFG spectrum. The experimental procedure is given in the Supporting Information. Since the SFG intensity arises from both nonresonant and resonant contributions, we fit the measured SFG intensity by using the simulated resonant parts of $\chi^{res,(2)}_{xxz}(\omega; r_t = 4 Å)$ and the fitting parameters $A_{NR}$, $\varphi_{NR}$, and $B$ as

$$I_{ssp}(\omega) \propto |A_{NR}e^{i\varphi_{NR}} + B\chi^{res,(2)}_{xxz}(\omega; r_t = 4Å)|^2 \quad (3)$$

where $A_{NR}$ is the nonresonant amplitude, $\varphi_{NR}$ is the nonresonant phase, and $B$ is the resonant amplitude. Since the librational mode peak at $\omega$ < 1000 $cm^{-1}$, making a non-negligible baseline change to the real part of the bending mode frequency, is enhanced by the cross-correlation term as seen in Figure 1 (c), $\chi^{res,(2)}_{xxz}$ $(\omega; r_t = 4 Å)$ is used for the fitting. The fitted SFG intensity spectrum is shown in Figure 2 with the experimentally measured spectrum. The nonresonant phase obtained from the fitting was −40°. The experimental data is well reproduced using the real and imaginary parts of the simulated resonant signal.

Having established good agreement between calculated and experimentally measured spectra of the bending mode, we can proceed to explore the molecular origin of the signal: which water molecules contribute to which part of the susceptibility? While the overall shape of the *ssp* spectrum reported here closely resembles that reported by Vinaykin and Benderskii,[15] we did not observe the shoulder at 1750 $cm^{-1}$, most likely the result of differences in experimental geometries (the incident angles of laser pulses are very different). To clarify the contributions of interfacial water with different HBs to the bend SFG signal, we decomposed the ensemble of the water molecules into subensembles with various amounts of the hydrogen-bonded donating H (DH) atom. The 0-, 1-, and 2-

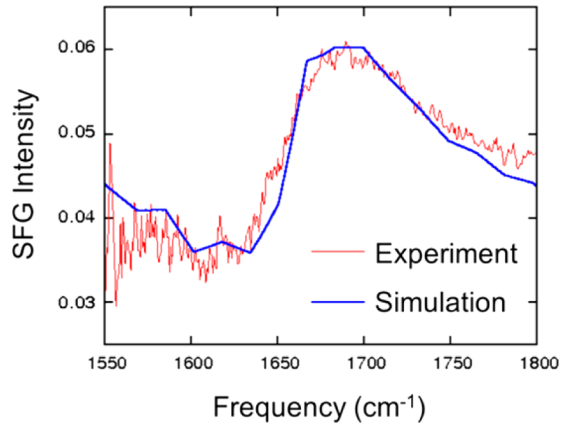


**Figure 2.** Experimentally measured SFG intensity (*ssp* polarization combination) and the fit from the simulated real and imaginary parts of $\chi^{res,(2)}_{xxz}(\omega; r_t = 4 Å)$ by using eq 3.

DH denote the molecules with two free O−H groups, one free O−H group one DH atom, and 2 DH atoms, respectively. We employed the HB definition based on the electronic occupancy of the O−H antibonding orbitals.[46] The axial distributions of these water molecules at the water−vapor interface are shown in Figure 3. In the bulk water region, the 2-DH water molecules are dominant, while the numbers of the 1-DH and 0-DH water molecules increase near the vapor region.

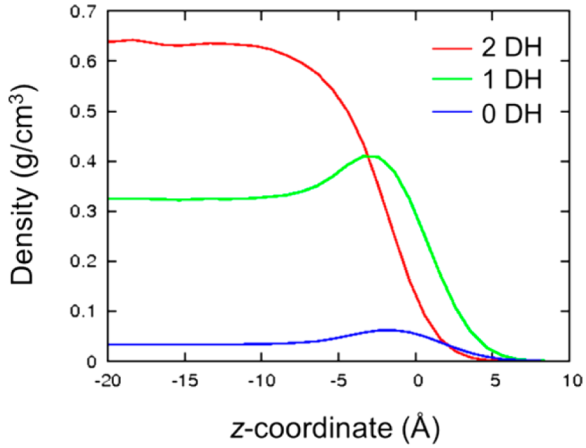


**Figure 3.** Axial distribution of the water density with different numbers of donor hydrogen atoms. The origin point is set to the Gibbs dividing surface, and $z$ > 0 and $z$ < 0 represent the vapor and bulk water regions, respectively.

As we are interested in the contribution of the free OH groups to the SFG bending mode signal, we have grouped in the following the 0-DH and 1-DH water molecules and compare this ensemble with the 2-DH ensemble (no free OH groups). Since the water bending mode resonant SFG spectrum is dominated by the autocorrelation terms as shown above, we use $\chi^{res,(2)}_{xxz}(\omega; r_t = 0 Å)$ to unravel the contributions of the different ensembles to the bending mode SFG spectrum. Moreover, without using cross-correlation terms, the response can be readily attributed to the (0/1)-DH and 2-DH water molecules. The SFG signals contributed by the $n'$-DH water molecules were calculated as


dx.doi.org/10.1021/jz400683v | J. Phys. Chem. Lett. 2013, 4, 1872−1877

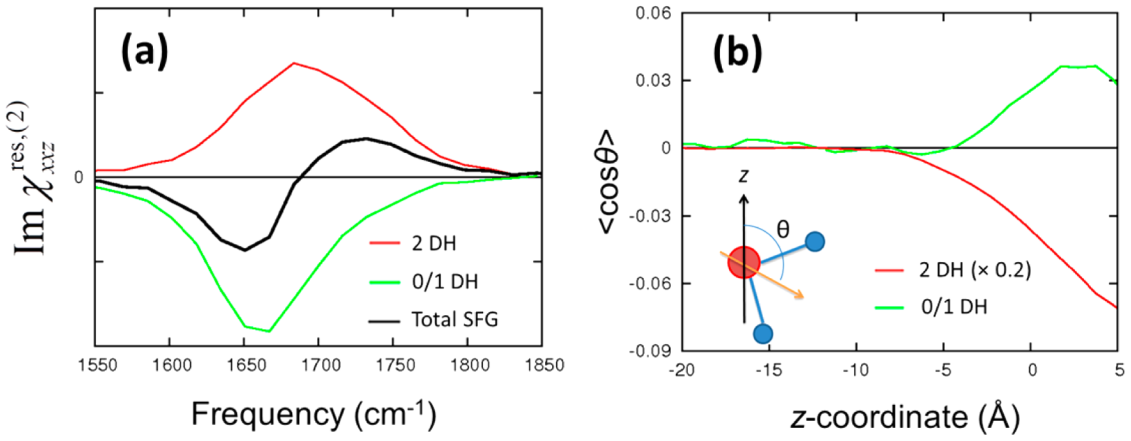


**Figure 4.** (a) Variations of the imaginary parts of the SFG responses, $\mathrm{Im}\chi^{res,n',(2)}_{xxz}(\omega; r_t = 0\ \text{Å})$ with different numbers of the donor hydrogen atoms. (b) Axial distributions of the angles formed by the surface normal and the bisector of the HOH angle. The origin point is set to the Gibbs dividing surface, and $z > 0$ and $z < 0$ represent the vapor and bulk water regions, respectively. The inset represents a schematic picture of the angle $\theta$ formed by the surface normal (black arrow) and the bisector of the HOH angle (orange colored arrow).

$$\chi^{res,n',(2)}_{xxz}(\omega; r_t) = iQ(\omega)\int_0^\infty dt e^{-i\omega t}\langle \sum_i g^3_{sc}(z_i(0))\mu_{i,z}(0)\alpha_{i,xx}(t)\delta_{n',n_i(0)}\rangle \quad (4)$$

where $\delta$ is the Kronecker delta and $n_i(t)$ is the number of donor HBs of water molecule $i$ at time $t$. The different contributions to the imaginary part of the SFG signals are shown in Figure 4a. The 2-DH water molecules exhibit a positive peak, while the 0/1-DH water molecules have a negative peak. The sign of the imaginary SFG susceptibility reflects the orientation of the transition dipole moment, but the relation is not a priori known. As the orientation of the HOH bending transition dipole is nearly parallel to the HOH angular bisector, we can obtain this relation by investigating the orientations of the HOH angular bisectors for water with different DH numbers. The axial distribution of the angles between the HOH angular bisector and the surface normal is plotted in Figure 4b. Note that the population data in Figure 3 determines the weights of this distribution. From Figure 4b it follows that the angular bisectors of the 2-DH water molecules on average point down to the bulk, while the bisectors of the 0/1-DH water molecules point up to the vapor region. Hence the sign of the HOH bending mode response and the HOH angular bisectors are anticorrelated. On the contrary, in the O−H stretching mode region, a positive SFG peak indicates that the O−H group and its transition dipole moment point up to the vapor region.[29] The sign of the imaginary part of the SFG spectra thus indicates an opposite direction of the transition dipoles of the HOH bending and the OH stretching modes.

Next, we focus on the frequencies of the peaks. The bending mode peak frequencies are 1660 and 1689 cm$^{-1}$ for the 0/1-, and 2-DH water molecules, respectively. As the HB number increases, the frequency of the HOH bending mode peak slightly increases. Since the average O−H stretch frequency decreases as the HB number increases, the frequency variations of the HOH bending and the O−H stretching modes show opposite tendency for the change of the HB number, which is consistent with eq 1. Moreover, the result indicates that the frequency of the HOH bending mode is not as sensitive to HBs as the O−H stretching mode. The positive SFG peak of the 2-DH water molecules and the negative peak contributed by the 0/1-DH water molecules separated by ∼29 cm$^{-1}$ interfere partially, resulting in a total SFG spectrum with a negative peak at ∼1650 cm$^{-1}$ and a positive peak at ∼1730 cm$^{-1}$.

The 2-DH water bending mode SFG peak is symmetric with a half width at half-maximum (HWHM) of 58 cm$^{-1}$, while the contribution to the SFG spectrum by the 0/1-DH water is asymmetric; in the lower frequency side of the peak ($\omega$ < 1660 cm$^{-1}$) the HWHM is 36 cm$^{-1}$, while at the higher frequency ($\omega$ > 1660 cm$^{-1}$) side the HWHM is 50 cm$^{-1}$. The asymmetry of the 0/1-DH water molecules' contribution presumably reflects the molecular asymmetry of the molecules containing both free and hydrogen-bonded OH groups, with different broadening mechanisms. Apparently, the symmetry-broken intermolecular interactions of the 1-DH water molecules affect the band shape for the HOH bend mode.

In summary, we have simulated the SFG susceptibility for the water bend mode at the water−vapor interface with the ab initio-based water model. The simulated water bend SFG intensity showed good agreement with the experimental data. The imaginary part of the overall SFG response shows a symmetric positive peak at ∼1730 cm$^{-1}$ and a negative peak at ∼1650 cm$^{-1}$. These peaks spaced by ∼80 cm$^{-1}$ arise from the interference of the 0/1-DH and 2-DH water contributions; the 0/1-DH water shows an asymmetric negative peak at 1660 cm$^{-1}$, while the 2-DH water shows a symmetric positive peak centered at 1689 cm$^{-1}$. The frequency difference of only 29 cm$^{-1}$ for the 0/1-DH and 2-DH water bending modes indicates that the water HOH bend frequency is relatively insensitive to the HB at the water−vapor interface in contrast to the high sensitivity of the O−H stretch mode. The signs of the peaks in the imaginary part of the SFG response provide information on the water orientations; a positive (negative) water bend SFG peak indicates that the water HOH angular bisector points down to the bulk (up to the vapor region). The simulated water bend SFG spectrum indicates that the HOH angular bisectors of the 0/1-DH and 2-DH water molecules orient up to the vapor region and down to the bulk region, respectively. The water bend SFG spectra provide information on the HOH angular bisector of an interfacial water molecule beyond the orientations of the OH groups which can be addressed by the OH stretch SFG spectra, leading to a full picture of interfacial water structures.


dx.doi.org/10.1021/jz400683v | J. Phys. Chem. Lett. 2013, 4, 1872−1877

## ■ ASSOCIATED CONTENT

### Supporting Information

Simulation details and experimental setup are described. This material is available free of charge via the Internet at http://pubs.acs.org.

## ■ AUTHOR INFORMATION


### Corresponding Author

*E-mail: nagata@mpip-mainz.mpg.de (Y.N.); bonn@mpip-mainz.mpg.de (M.B.).


### Notes

The authors declare no competing financial interest.

## ■ ACKNOWLEDGMENTS

We are grateful to Dr. M. Morita and Dr. K. Takahashi for fruitful discussions. C.-S.H. acknowledges the financial support from the Nederlandse Organisatie voor Wetenschappelijk Onderzoek.

## ■ REFERENCES


(1) Ball, P. Water as an Active Constituent in Cell Biology. *Chem. Rev.* **2008**, *108*, 74−108.

(2) Patankar, N. A. Mimicking the Lotus Effect: Influence of Double Roughness Structures and Slender Pillars. *Langmuir* **2004**, *20*, 8209−8213.

(3) Dorrer, C.; Rühe, J. Some Thoughts on Superhydrophobic Wetting. *Soft Matter* **2008**, *5*, 51−61.

(4) D'Acunzi, M.; Mammen, L.; Singh, M.; Deng, X.; Roth, M.; Auernhammer, G. K.; Butt, H. J.; Vollmer, D. Superhydrophobic Surfaces by Hybrid Raspberry-like Particles. *Faraday Discuss.* **2010**, *146*, 35−48.

(5) Deng, X.; Mammen, L.; Butt, H. J.; Vollmer, D. Candle Soot as a Template for a Transparent Robust Superamphiphobic Coating. *Science* **2012**, *335*, 67−70.

(6) Shen, Y. R. *The Principles of Nonlinear Optics*; Wiley-Interscience: New York, 1984.

(7) Morita, A.; Hynes, J. T. A Theoretical Analysis of the Sum Frequency Generation Spectrum of the Water Surface. *Chem. Phys.* **2000**, *258*, 371−390.

(8) Du, Q.; Freysz, E.; Shen, Y. R. Vibrational Spectra of Water Molecules at Quartz/Water Interfaces. *Phys. Rev. Lett.* **1994**, *72*, 238−241.

(9) Sovago, M.; Campen, R. K.; Wurpel, G. W. H.; Müller, M.; Bakker, H. J.; Bonn, M. Vibrational Response of Hydrogen-Bonded Interfacial Water Is Dominated by Intramolecular Coupling. *Phys. Rev. Lett.* **2008**, *100*, 173901.

(10) Nihonyanagi, S.; Ishiyama, T.; Lee, T.-K.; Yamaguchi, S.; Bonn, M.; Morita, A.; Tahara, T. Unified Molecular View of the Air/Water Interface Based on Experimental and Theoretical $\chi^{(2)}$ Spectra of an Isotopically Diluted Water Surface. *J. Am. Chem. Soc.* **2011**, *133*, 16875−16880.

(11) Scatena, L. F.; Brown, M. G.; Richmond, G. L. Water at Hydrophobic Surfaces: Weak Hydrogen Bonding and Strong Orientation Effects. *Science* **2001**, *292*, 908−912.

(12) Stiopkin, I. V.; Weeraman, C.; Pieniazek, P. A.; Shalhout, F. A.; Skinner, J. L.; Benderskii, A. V. Hydrogen Bonding at the Water Surface Revealed by Isotopic Dilution Spectroscopy. *Nature* **2011**, *474*, 192−195.

(13) Nagata, Y.; Pool, R. E.; Backus, E. H. G.; Bonn, M. Nuclear Quantum Effects Affect Bond Orientation of Water at the Water−Vapor Interface. *Phys. Rev. Lett.* **2012**, *109*, 226101.

(14) Liu, J.; Andino, R. S.; Miller, C. M.; Chen, X.; Wilkins, D. M.; Ceriotti, M.; Manolopoulos, D. E. A Surface-Specific Isotope Effect in Mixtures of Light and Heavy Water. *J. Phys. Chem. C* **2013**, *117*, 2944−2951.

(15) Vinaykin, M.; Benderskii, A. V. Vibrational Sum-Frequency Spectrum of the Water Bend at the Air/Water Interface. *J. Phys. Chem. Lett.* **2012**, *3*, 3348−3352.

(16) Isaienko, O.; Nihonyanagi, S.; Sil, D.; Borguet, E. Observation of the Bending Mode of Interfacial Water at Silica Surfaces by Near-Infrared Vibrational Sum-Frequency Generation Spectroscopy of the [Stretch + Bend] Combination Bands. *J. Phys. Chem. Lett.* **2013**, *4*, 531−535.

(17) Rey, R.; Møller, K. B.; Hynes, J. T. Ultrafast Vibrational Population Dynamics of Water and Related Systems: A Theoretical Perspective. *Chem. Rev.* **2004**, *104*, 1915−1928.

(18) Larsen, O. F. A.; Woutersen, S. Vibrational Relaxation of the $H_2O$ Bending Mode in Liquid Water. *J. Chem. Phys.* **2004**, *121*, 12143−12145.

(19) Rey, R.; Ingrosso, F.; Elsaesser, T.; Hynes, J. T. Pathways for $H_2O$ Bend Vibrational Relaxation in Liquid Water. *J. Phys. Chem. A* **2009**, *113*, 8949−8962.

(20) Ashihara, S.; Huse, N.; Espagne, A.; Nibbering, E. T. J.; Elsaesser, T. Ultrafast Structural Dynamics of Water Induced by Dissipation of Vibrational Energy. *J. Phys. Chem. A* **2007**, *111*, 743−746.

(21) McGuire, J. A.; Shen, Y. R. Ultrafast Vibrational Dynamics at Water Interfaces. *Science* **2006**, *313*, 1945−1948.

(22) Smits, M.; Ghosh, A.; Sterrer, M.; Müller, M.; Bonn, M. Ultrafast Vibrational Energy Transfer between Surface and Bulk Water at the Air−Water Interface. *Phys. Rev. Lett.* **2007**, *98*, 098302.

(23) Ghosh, A.; Smits, M.; Bredenbeck, J.; Bonn, M. Membrane-Bound Water Is Energetically Decoupled From Nearby Bulk Water: An Ultrafast Surface-Specific Investigation. *J. Am. Chem. Soc.* **2007**, *129*, 9608−9609.

(24) Eftekhari-Bafrooei, A.; Borguet, E. Effect of Surface Charge on the Vibrational Dynamics of Interfacial Water. *J. Am. Chem. Soc.* **2009**, *131*, 12034−12035.

(25) Zhang, Z.; Piatkowski, L.; Bakker, H. J.; Bonn, M. Ultrafast Vibrational Energy Transfer at the Water/Air Interface Revealed by Two-Dimensional Surface Vibrational Spectroscopy. *Nat. Chem.* **2011**, *3*, 888−893.

(26) Hsieh, C. −S.; Campen, R. K.; Vila Verde, A. C.; Bolhuis, P.; Nienhuys, H. −K.; Bonn, M. Ultrafast Reorientation of Dangling OH Groups at the Air−Water Interface Using Femtosecond Vibrational Spectroscopy. *Phys. Rev. Lett.* **2011**, *107*, 116102.

(27) Xiong, W.; Laaser, J. E.; Mehlenbacher, R. D.; Zanni, M. T. Adding a Dimension to the Infrared Spectra of Interfaces using Heterodyne Detected 2D Sum-Frequency Generation (HD 2D SFG) Spectroscopy. *Proc. Natl. Acad. Sci. U.S.A.* **2011**, *108*, 20902−20907.

(28) Falk, M. The Frequency of the H−O−H Bending Fundamental in Solids and Liquids. *Spectrochim. Acta, Part A* **1984**, *40*, 43−48.

(29) Morita, A.; Hynes, J. T. A Theoretical Analysis of the Sum Frequency Generation Spectrum of the Water Surface. II. Time-Dependent Approach. *J. Phys. Chem. B* **2002**, *106*, 673−685.

(30) Ishiyama, T.; Morita, A. Analysis of Anisotropic Local Field in Sum Frequency Generation Spectroscopy with the Charge Response Kernel Water Model. *J. Chem. Phys.* **2009**, *131*, 244714.

(31) Ishiyama, T.; Morita, A. Vibrational Spectroscopic Response of Intermolecular Orientational Correlation at the Water Surface. *J. Phys. Chem. C* **2009**, *113*, 16299−16302.

(32) Nagata, Y.; Mukamel, S. Vibrational Sum-Frequency Generation Spectroscopy at the Water/Lipid Interface: Molecular Dynamics Simulation Study. *J. Am. Chem. Soc.* **2010**, *132*, 6434−6442.

(33) Nagata, Y.; Mukamel, S. Spectral Diffusion at the Water/Lipid Interface Revealed by Two-Dimensional Fourth-Order Optical Spectroscopy: A Classical Simulation Study. *J. Am. Chem. Soc.* **2011**, *133*, 3276−3279.

(34) Pieniazek, P. A.; Tainter, C. J.; Skinner, J. L. Interpretation of the Water Surface Vibrational Sum-Frequency Spectrum. *J. Chem. Phys.* **2011**, *135*, 044701.

(35) Pieniazek, P. A.; Tainter, C. J.; Skinner, J. L. Surface of Liquid Water: Three-Body Interactions and Vibrational Sum-Frequency Spectroscopy. *J. Am. Chem. Soc.* **2011**, *133*, 10360−10363.

(36) Ni, Y.; Gruenbaum, S. M.; Skinner, J. L. Slow Hydrogen-Bond Switching Dynamics at the Water Surface Revealed by Theoretical Two-Dimensional Sum-Frequency Spectroscopy. *Proc. Natl. Acad. Sci. U.S.A.* **2013**, *110*, 1992−1998.
(37) Sulpizi, M.; Salanne, M.; Sprik, M.; Gaigeot, M.-P. Vibrational Sum Frequency Generation Spectroscopy of the Water Liquid−Vapor Interface from Density Functional Theory-Based Molecular Dynamics Simulations. *J. Phys. Chem. Lett.* **2013**, *4*, 83−87.
(38) Vila Verde, A. C.; Bolhuis, P. G.; Campen, R. K. Statics and Dynamics of Free and Hydrogen-Bonded OH Groups at the Air/Water Interface. *J. Phys. Chem. B* **2012**, *116*, 9467−9481.
(39) Perry, A.; Ahlborn, H.; Space, B.; Moore, P. B. A Combined Time Correlation Function and Instantaneous Normal Mode Study of the Sum Frequency Generation Spectroscopy of the Water/Vapor Interface. *J. Chem. Phys.* **2003**, *118*, 8411−8419.
(40) Perry, A.; Neipert, C.; Ridley, C.; Space, B.; Moore, P. B. Identification of a Wagging Vibrational Mode of Water Molecules at the Water/Vapor Interface. *Phys. Rev. E* **2005**, *71*, 050601.
(41) Perry, A.; Neipert, C.; Ridley, C.; Green, T.; Space, B.; Moore, P. B. A Theoretical Description of the Polarization Dependence of the Sum Frequency Generation Spectroscopy of the Water/Vapor Interface. *J. Chem. Phys.* **2005**, *123*, 144705.
(42) Hasegawa, T.; Tanimura, Y. A Polarizable Water Model for Intramolecular and Intermolecular Vibrational Spectroscopies. *J. Phys. Chem. B* **2011**, *115*, 5545−5553.
(43) Imoto, S.; Xntheas, S. S.; Saito, S. Molecular Origin of the Difference in the HOH Bend of the IR Spectra between Liquid Water and Ice. *J. Chem. Phys.* **2013**, *138*, 054506.
(44) Egorov, S. A.; Skinner, J. L. Semiclassical Approximations to Quantum Time Correlation Functions. *Chem. Phys. Lett.* **1998**, *293*, 469−476.
(45) Cho, M.; Fleming, G. R.; Saito, S.; Ohmine, I.; Stratt, R. M. Instantaneous Normal Mode Analysis of Liquid Water. *J. Chem. Phys.* **1994**, *100*, 6672−6683.
(46) Kumar, R.; Schmidt, J. R.; Skinner, J. L. Hydrogen Bonding Definitions and Dynamics in Liquid Water. *J. Chem. Phys.* **2007**, *126*, 204107.